Earth Surf. Dynam. Discuss., https://doi.org/10.5194/esurf-2018-66
Manuscript under review for journal Earth Surf. Dynam.
Discussion started: 19 September 2018

Earth Surface Dynamics Discussions
Open Access
EGU

Observations and scaling of tidal mass transport across the lower Ganges-Brahmaputra delta plain: implications for delta management and sustainability

Richard Hale[1], Rachel Bain[2], Steven Goodbred Jr.[2], Jim Best[3]
[1]Dept. of Ocean, Earth, and Atmos. Sci., Old Dominion University, Norfolk, VA, USA
[2]Earth and Environmental Sciences Dept., Vanderbilt University, Nashville, TN USA
[3]Departments of Geology, Geography & GIS, Mechanical Science and Engineering and Ven Te Chow Hydrosystems Laboratory, University of Illinois, Champagne, IL USA

Abstract

The landscape of southwest Bangladesh, a region constructed primarily by fluvial processes associated with the Ganges and Brahmaputra Rivers, is now maintained almost exclusively by tidal processes as the fluvial system has migrated to the east through the Holocene. In natural areas such as the Sundarbans National Forest, year-round spring-tide inundation delivers sufficient sediment for vertical accretion to keep pace with relative sea-level rise. However, recent human modification of the landscape in the form of embankment construction has terminated this pathway of sediment delivery for much of the region, resulting in a startling elevation imbalance, with inhabited areas often sitting >1 m below mean high water. Restoring this landscape, or preventing land loss in the natural system, requires an understanding of how rates of water and sediment flux vary across time scales ranging from hours to months. In this study, we combine time-series observations of water level, salinity, and suspended sediment concentration, with ship-based measurements of large tidal channel hydrodynamics and sediment transport. To capture the greatest possible range of variability, cross-channel transects designed to encompass a 12.4-h tidal cycle were performed in both dry and wet seasons, during spring and neap tides.

Regional suspended sediment concentration begins to increase in August, coincident with a decrease in local salinity, indicating the arrival of the sediment-laden, freshwater plume of the combined Ganges-Brahmaputra-Meghna rivers. We observe profound seasonality in sediment transport, despite somewhat modest seasonal variability in the magnitude of water discharge, indicating the importance of this seasonal sediment delivery. On tidal time-scales, spring tides transport an order of magnitude more sediment than neap tides in both the wet and dry seasons. In aggregate, sediment transport is flood-oriented, likely a result of tidal pumping. Finally, we note that rates of sediment and water discharge in the tidal channels are of the same scale as the annually averaged values for the Ganges or Brahmaputra rivers. These observations provide context for examining the relative importance of fluvial and tidal processes in what has been defined as the quintessential tidal delta in the classification scheme of Galloway. These data also inform critical questions regarding the timing and magnitude of sediment delivery to the region, which are especially important in predicting, and preparing for, future change under changing environmental conditions.

Earth Surf. Dynam. Discuss., https://doi.org/10.5194/esurf-2018-66
Manuscript under review for journal Earth Surf. Dynam.
Discussion started: 19 September 2018

1 – Introduction

The world's great deltas are currently threatened by a variety of factors, including global sea level rise (Overeem and Syvitski, 2009), overpopulation (Ericson et al., 2006), changes in sediment supply (Syvitski 2003; Syvitski and Milliman, 2007; Anthony et al., 2015; Darby et al., 2016), and other human-related activities such as water diversions, flood control structures, and groundwater and hydrocarbon extraction (Syvitski et al., 2009). The Ganges-Brahmaputra-Meghna (GBM) delta is one of the most heavily populated regions that is undergoing locally accelerated sea-level rise (~0.5 cm/y; Higgins et al., 2014) due to a combination of natural and anthropogenic factors including eustatic sea-level change, tectonic subsidence, fine-grained sediment compaction, and groundwater extraction (Overeem and Syvitski, 2009; Syvitski, 2008; Steckler et al., 2010). In addition, when factors like tidal amplification due to anthropogenic reworking of the distributary channel network are considered, the relative rate of sea-level rise can exceed 1.6 cm/yr (Pethick and Orford, 2013). Furthermore, the future viability of the delta is threatened by the proposed construction of dams and water diversions associated with the India River Linking Project, which, if completed as proposed, could drastically reduce sediment delivery to Bangladesh (Higgins et al., 2018).

Restoration of land-surface elevation in many populated areas in the GBM delta is already necessary due to the relative loss in elevation that has occurred since the widespread construction of embankments during the 1960s to 1980s. Both planned (tidal river management) and unplanned (embankment failures) flooding of local polders (the embanked islands) has demonstrated the capacity of the natural system for effective sediment transport and deposition, with decimeters of annual accretion observed during recent breach events (Khadim et al., 2013; Auerbach et al., 2015; Kamal et al., 2017; Darby et al., 2018). One of the most important strategies that has been forwarded to reduce the threat of unintended inundations in SW Bangladesh is a plan for polder management (Brammer, 2014). However, many questions concerning potential management strategies remain, not the least of which are an accurate quantification of total available sediment mass and an understanding of the tidal processes involved in its transport and deposition. Toward these goals, the present study provides observation-based calculations of water and sediment transport through a major tidal channel in the delta across spring-neap tidal cycles and seasonal time scales, with the goal of identifying the timing and magnitude of mass sediment exchange between the different tidal channels. These results are then considered in the context of prior research concerning sediment accumulation and rates of channel infilling to better understand the role of tidal mass transport within the lower GBM delta plain.

2 – Background

Much of the low-lying coastal region of SW Bangladesh is under threat of long-term inundation (Auerbach et al., 2015; Brown and Nicholls, 2015). The risk is particularly acute for islands that were embanked ("poldered") in the 1960s and 1970s as part of a program designed to increase the area of arable land through the prevention of tidal inundation in agricultural areas (Islam, 2006; Nowreen et al., 2014). Approximately 5000 km of polder

embankments were built by hand, generating 9000 km^2 of new farmland, but also eliminating the semi-diurnal exchange of water and sediment between the tidal channels and tidal platform (Islam, 2006; Nowreen et al., 2014). As a result, sediment resupply pathways have been effectively terminated and the former floodplain surface in these regions now lies 1.0-1.5 m below mean high water due to a combination of sediment starvation, enhanced sediment compaction, and tidal-range amplification (Auerbach et al., 2015; Pethick and Orford, 2013).

In contrast to the poldered landscape, the adjacent mangrove system of the Sundarbans National Forest (SNF) is primarily inundated during spring high tides, and its sedimentation and vegetation are keeping pace with sea-level rise (Rogers et al., 2013; Auerbach et al., 2015;). Protecting the SNF is of critical importance, as coastal wetlands and mangroves provide irreplaceable ecosystem services including storm-surge buffering (Uddin et al., 2013; Marois and Mitsch, 2015; Hossain et al., 2016; Sakib et al., 2015), serving as effective carbon traps (Mcleod et al., 2011; Alongi, 2012; Pendleton et al., 2012) and perhaps even helping to combat the impacts of ocean acidification (Yan, 2016).

For the GBM delta, a unit-scale analysis of mass balance (Rogers et al., 2013) suggests that the annual sediment load of the GBM river system (~1.1 Gt/y) is sufficient to aggrade the entire delta system at rates ≥ 0.5 cm/yr, and thus provides potential to keep pace with moderately high rates of sea-level rise. Such aggradation, of course, requires effective dispersal of riverine sediment to disparate regions of the delta. Recent research suggests a close coupling of discharge at the river mouth to sediment deposition in the remote delta plain by way of tidal exchange (Allison and Kepple, 2001; Rogers et al., 2013; Auerbach et al., 2015; Wilson et al., 2017). Such tidally supported sedimentation yields mean accretion rates of ~1 cm/ yr, with local observations regularly reaching 3-5 cm/yr, which together indicate robust sediment delivery to the Sundarbans and SW coastal region (Rogers et al., 2013). Thus, as the principal conduit for sediment that can maintain the elevation of this region, an understanding and quantification of the tidal water and sediment exchange is essential to foresee future impacts of accelerated sea-level rise and the potential for mitigation.

3 – Methods

3.1 – Study Area

Our research concerns a network of tidal channels located approximately 80 km from the coast along the Pussur River system, itself one of five similarly sized tidal distributary networks (Fig. 1). Tidal exchange extends >120 km inland of the coast along the Pussur River, with one branch ultimately connecting to the Gorai River, a distributary of the mainstem Ganges River (Fig. 1). The tidal range along the Pussur River approaches its maximum in the study area at 4-5 m for the spring tidal range, as compared with 3-3.5 m on the coast at Hiron Point. The area is also societally relevant, lying at the transition from the pristine Sundarbans to the embanked polders, and near the formerly active shipping port of Mongla and cyclone- and flood- impacted island of Polder 32 (labelled P32 on Fig. 1; Auerbach et al., 2015).

Within this area, our observations were collected in the primary tidal channel of the Shibsa River and two of its major bifurcations that connect with the Pussur channel, the Dhaki River and Bhadra River (Fig. 1). The Shibsa River is the largest of these channels, with local widths of 1-2 km, compared to 0.25-0.8 km and 0.15-0.3 km, for the Dhaki and Bhadra Rivers, respectively. At its eastern extent, the Dhaki River connects to the Pussur River, serving as the first major cross-channel to link the Shibsa and Pussur River channels after they bifurcate ~60 km to the south (Fig. 1). At its upstream extent, the Pussur tidal channel connects with the downstream mouth of the Gorai River, which delivers a water discharge of ~3000 m^3/s during the monsoon season to ~0 m^3/s during the dry season (Winterwerp and Giardino, 2012). Salinity in the study area ranges from 0-1 PSU during the monsoon, to 20-30 PSU during the dry season (Shaha and Cho, 2016; Ayers et al., 2018). This seasonal variation in salinity is controlled by local runoff, the freshwater discharge from the Gorai River, and to a much larger extent, the magnitude of the regional plume of the GBM rivers (Rogers et al., 2013).

3.2. – Hydrodynamic Observations

To establish tidal stage and capture surface-water elevations during the hydrodynamic surveys, pressure sensors were deployed at multiple locations across the study area (Fig. 1). All sensors were deployed as close to low water as possible and recorded at 5- or 10-minute intervals. Periods of subaerial sensor exposure (of up to 150 minutes at low tide) were interpolated using a robust ordinary least-squares method provided by Grinsted (2008). The agreement between measurement and prediction was generally good, with predicted range being 0.98 of the measured range for a given time period, thus suggesting that the interpolated data are both reasonable and conservative. The values reported herein are of the interpolated values. Tidal range, water temperature, and conductivity have also been monitored continuously since 2014 at the Sutarkhali station (Fig. 1B), with an optical backscatter sensor (OBS) to measure suspended sediment concentration (SSC) added in late March 2015. While the sediment concentrations recorded by this near-bed instrument are not directly comparable to the depth-averaged measurements made during the present cross-channel surveys, we herein use these data to extend our understanding of system behavior between the dry and monsoon seasons. For broader context, data from the sensors deployed at the Sutarkhali station are also compared to monthly averaged water discharge for the Ganges and Brahmaputra rivers for the period 1980-2000, based on data from the Bangladesh Water Development Board, and Ganges River sediment discharge data digitized from Lupker et al. (2011).

To quantify water and sediment flux in this area of the tidal transport system, cross-channel hydrodynamic surveys were conducted during spring and neap tidal conditions at two transects on the Shibsa River during the dry (March 2015) and wet (August/September 2015) seasons. An additional wet season transect was also conducted during moderate tides on the Pussur River. On the Shibsa River, the southern transect was located south of the poldered landscape and entirely within the confines of the SNF (Fig.1). The northern transect was located ~12 km upstream in the poldered region, just south of the Dhaki-Shibsa confluence and adjacent to Polder 32 to the east and Polder 10-12 to the west (Fig. 1B). Two secondary channels are present between these transect locations that

185 divert water onto the Sundarbans tidal platform and associated creek network. Dry season
186 surveys at both the southern and northern transects took place during peak neap (15-16
187 Mar) and spring (21-22 Mar) tides. During the ensuing monsoon season, spring tides were
188 measured on August 30-31 (southern transect) and September 2 (northern transect),
189 followed by neap tides on September 7 and 8 (northern and southern transects,
190 respectively). Surveys lasted for 11-13 hours as conditions allowed, encompassing
191 approximately one-half of a tidal cycle (i.e., one high and one low tide). Because this system
192 is largely semi-diurnal with a minimal mixed component, we are confident that this time
193 interval was long enough to describe the system dynamics accurately.
194
195 The surveys were conducted using Sontek M9 multi-frequency ADCP's to collect flow-
196 perpendicular observations of current velocity and direction. Data were collected at 1 Hz,
197 using both 1.0 and 3.0 MHz transducers, resulting in vertical bins ranging in height from
198 0.1-1.0 m. From these values, total discharge was calculated by integrating velocity over
199 space and time. River conventions are used for presenting velocity and discharge data,
200 where positive values refer to the ebb or downstream direction and negative values for the
201 flood or upstream transport. A typical survey day included 50-60 individual river crossings
202 at the transect location, measuring cumulative discharge in both directions across the
203 channel. Because surveys could only be conducted during daylight hours and as weather
204 conditions allowed, discharge is interpolated to complete a 12.4-hour tidal cycle, which is
205 the average tidal cycle duration in the area (range: 11.9-13.1 h). By assuming that the
206 change in tidal prism is negligible between consecutive tides, as suggested by the similarity
207 in tidal elevations (Fig. 2), we can tile measurements in 12.4 h increments and interpolate
208 using a cubic spline. Working conditions were particularly challenging during the monsoon
209 season, resulting in especially short-duration survey days. In the absence of measured
210 discharge, we use a mass balance approach to constrain the magnitude of the missing tidal
211 prism data. For the monsoon-season spring tides, we treat the region between the southern
212 and northern transects and the southern Bhadra River as a closed system with no long-
213 term (>1 semidiurnal period) water storage. Using measured Bhadra River discharge
214 values and assuming a negligible to slightly southerly-directed net flux through the
215 adjacent Sundarbans, allows us to determine the likely range of values for the unmeasured
216 ebb prism at the southern transect. For the monsoon-season neap tides, we consider the
217 larger region bounded by the southern transect to the southwest, the Pussur River below
218 the Dhaki River confluence to the southwest, and the Bangladesh Water Development
219 Board gauging station at the Gorai Railway Bridge ~275 river km to the north. Balancing
220 the measured net flux through the Pussur River and the recorded upstream discharge of
221 the Gorai River of 3000 m^3/s with the measured ebb prism at the southern transect allows
222 us to estimate the missing southern transect flood prism. We then repeated this spring tide
223 procedure to estimate the unmeasured neap flood prism at the northern transect.
224
225 **3.3 – Sediment Observations**
226
227 In addition to water discharge, observations of SSC along the transect lines were made
228 using a combination of filtered water samples and optical-backscatter (OBS)
229 measurements. While the exact sampling method varied depending on available
230 instrumentation and river conditions, the general approach involved collecting OBS

profiles to the maximum possible depth (<10 m), at either two (northern transect) or three (southern transect) locations along the channel edges and centerline (Fig. 1). OBS measurements were supplemented by simultaneous water samples (100-200 ml) collected from various depths using a Niskin sampler. Water samples were filtered using pre-weighed 0.4-μm nitrocellulose filters and washed with freshwater to remove salts. The filters were then dried overnight and re-weighed to determine the volume-concentration of sediment. The OBS measurements were calibrated by comparing the voltage response observed in the field with the measured concentrations from the same time and location, in a method modified from Ogston and Sternberg (1999). Correlation between filtered samples and instrument voltage was strong, with an average r-squared value of 0.83±0.1.

In order to calculate the total sediment fluxes, the vertically and horizontally distributed SSC observations collected for each channel cross-section were averaged to produce a series of temporally discrete SSC values over the course of one tidal cycle. This spatial averaging appears suitable because the variance was considerably smaller than the temporal variability associated with tidal discharge and strong seasonal contrasts. Using wet season data as an example, the average standard deviation of SSC through time at one sample location was 0.2 g/L, while the average standard deviation of SSC between stations at any given time was 0.13 g/L. When conditions did not allow samples to be collected at depths below the water surface, a scaling factor of 1.25 was applied to account for the higher sub-surface SSC, which we determined by the relationship between depth-averaged concentrations and surface concentrations from the other available data. Similarly, measurements from 15 March (dry-season neap tide) were only collected at depths of 5 and 15 m and were thus scaled by a factor of 0.81 to be comparable to other measurements that included surface SSC values. An important caveat for all SSC measurements is that we are referring primarily to suspended load, largely ignoring the bedload component. While this is presumably a measurable component of the total sediment transport, bedload is likely unable to exit the tidal channels during platform irrigation, and as such is not considered an important source of sediment for land construction. As with our measurements of water discharge, SSC values were calculated over an entire tidal cycle by tiling observations in 12.4-hour segments and interpolating using a cubic spline. From these values, the integrated product of water discharge and SSC yields net sediment flux, which we compute using the time series for each component as calculated using the aforementioned methods.

4 – Results

4.1 – Long-term Pressure and OBS:

At our long-term station deployed in a secondary tidal channel (Fig. 1), recorded water-level variations show tidal-period excursions with a range of 1.8 to 4.8 m over the 12 months of observation (Fig. 2). This variance is, of course, driven primarily by the fortnightly spring-neap tidal cycle, but there is also a seasonal variability showing the monsoon period to have a reduced tidal range as compared with the dry season. In this case, the neap tidal range is ~10% less during the monsoon season, and the spring tidal

range is as much ~20% less, accounting for a nearly 1 m difference (3.9 m vs. 4.8 m). This reduced range in the monsoon season, however, is not manifested in the elevation of high-tide water levels, which remained largely consistent between seasons. Rather, the difference is caused by higher water levels during low tide (Fig. 2), which has the effect of truncating the tidal range and yielding an overall higher mean water level. These higher low-water levels associated with the monsoon suggest that they are tied to regional freshwater drainage and discharge. In addition, another contributing factor could be the seasonally reversing wind stresses, but such set-up should enhance high water levels as well, suggesting that they are not the primary cause. Although further research on this topic is needed, these distinctions are important herein for understanding the behavior of the tidal delta plain, as landscape elevations in this region are closely tied to mean high-tide water levels, and not mean sea level (Auerbach et al., 2015). Thus, as first demonstrated by Pethick and Orford (2013), the monthly mean tide-gauge data often used to track seasonal to interannual variations in water level may have relatively little bearing on the tidal inundation period and sedimentation rates that control tidal platform elevation (Rogers et al. 2013).

The arrival of fully freshwater (wet-season) conditions occurs in July, following the peak in Brahmaputra River water discharge, and roughly coincident with peak Ganges River water discharge (Fig. 3). Coupled with our long-term pressure gauge, the OBS sensor recorded relatively constant, but low, mean SSC from the late dry season into the early monsoon period (late March through July), with weak but noticeable spring-neap variability ranging from ~0.01 g/L to 0.20 g/L (Fig. 2). However, moving into peak monsoon season, SSC increases markedly from early August through September, concurrent with the Ganges River sediment discharge peak (Figs. 2, 3). Individual measurements regularly exceeded 0.50 g/L during this time, with maxima >2.5 g/L (Fig. 2). SSC variability around the semi-diurnal tide and spring-neap cycles was greatly enhanced compared with that during the dry season, with SSC values during spring tidal cycles exceeding those observed during neap conditions by a factor of 2-10. By the end of observations in October 2015, SSC began to drop to levels similar to those observed in mid-August (0.01-1.0 g/L; Fig. 2), but on average remained well above those of the dry season. For comparison, the mean annual SSC of the mainstem Ganges-Brahmaputra river is ~1 g/L, and depth-averaged values in the main estuary mouth and on the inner shelf commonly range 2-5 g/L during high river discharge (Barua et al., 1994; Ali et al., 2013). In total, SSC values well in excess of 1 g/L are regularly observed during the wet season from the mainstem river to the inner shelf and into the tidal channels of the lower delta plain. These results support previous evidence for the strong coupling of seasonal river discharge with penecontemporaneous sedimentation in the remote tidal delta plain (Rogers et al., 2013).

4.2 – Hydrography – Water Discharge:

Dry season tidal range on the Shibsa River, as measured at Nalian near the northern transect (Fig. 1B), varied from 2.3 m during the neap minima to 5.6 m during spring maxima (Fig. 2). The tidal period was slightly longer during neap tides than spring tides (12.9 h vs. 12.3 h), and the mixed component of the semi-diurnal tide was more pronounced, with consecutive tidal ranges varying by as much as 0.55 m during neap tides,

versus 0.23 m during spring tides (Fig. 2). During the monsoon fieldwork, the tidal range was 2.4 and 4.2 m for the neap and spring tides respectively. As with the dry season, total tidal period during neap tides was slightly longer than spring tides (12.8 h vs. 12.0 h). The mixed semi-diurnal variability was again greater during neap tides as well, which varied by as much as 0.25 m, while spring tide variability was typically <0.10 m (Fig. 2).

In order to calculate the dry-season tidal prism (i.e., integrated ebb and flood discharges), our observations captured both peak flood and ebb discharges, with interpolation being used over the remaining <5-15% of the tidal cycle (Fig. 4). During the monsoon season, challenging field conditions resulted in several surveys capturing only a partial tidal cycle (~8-9 hr survey; Fig. 4). Only during northern transect spring tides were conditions favorable for collecting observations of similar duration to the dry season (~11 hr survey; Fig. 4). Within these limits, however, we have used conservative interpolation to generate error-bound estimates of total water discharge, the resulting patterns of which provide robust observations concerning system behavior (see Section 2; Fig. 4).

The average tidal prism magnitudes for the northern and southern transects are $2.1\pm0.7 \times 10^8$ m^3 and $3.4\pm1.4 \times 10^8$ m^3, respectively. Included in these averages the absolute values of flood and ebb tidal prisms measured on spring and neap tides during both wet and dry seasons (Table 1). Thus, the tidal prism at the northern transect averages only ~60±10% that of the southern transect regardless of season, even though they are located just 10 km apart. Most of this difference in discharge (*c.* 80-100%) can be balanced by water storage between the two locations, where the product of tidal range and area between transects is *c.* 6.7×10^7 m^3. Considering differences in seasonal discharge, results show that the neap ebb prism is ~30% greater during the monsoon at both transects, despite having a smaller tidal range compared with the dry season survey. This difference of $4\text{-}6 \times 10^7$ m^3 equates to an excess ebb discharge of 1800-2800 m^3/s, which is about 45-70% of the mean monsoon discharge of the upstream Gorai river. We thus take the greater wet-season ebb prism to simply reflect the addition of local freshwater discharge from the Gorai River (Table 1; Fig. 1).

Strictly speaking, defining a tidal regime as either ebb- or flood- dominant refers to the water velocity rather than discharge (Pethick, 1980; Brown and Davies, 2010). In the present study, however, we are interested in the net movement of water and sediment and thus refer to a particular discharge regime as either ebb or flood "dominated" or "oriented" based on the net tidal prism (i.e., the difference between ebb and flood discharge). With this in mind, our surveys suggest that the system varies between ebb and flood orientation across both tidal phase and season (Table 1). For example, both transects during the dry, spring and wet, neap surveys show the average ebb-tidal prism to be 26±16% larger than the flood limb. In contrast, the other two survey periods (dry, neap and wet, spring) yielded balanced to slightly flood dominated tidal prisms (9±8%). In summary, although our results on water balance are insufficient for a full understanding of the patterns, a key finding is that the ebb and flood tidal prisms rarely balance at this location. These tidal-prism asymmetries appear to be a salient characteristic of the complex, interconnected channel network of the GBMD tidal delta plain. Thus, even our limited observations require

a lateral (east-west) exchange of water between the Shibsa and parallel Pussur channels (Fig. 1), which we presume to be driven by locally non-uniform tidal phasing within the channel network. Given these emergent circulation patterns, it is clear that individual channels do not operate as closed systems and exhibit local, non-uniform mass exchange, providing a first indication of how morphologic evolution of the tidal delta plain occurs.

Although the relative dominance between the ebb and flood tidal prisms covaries persistently (as described above), the mean and instantaneous water discharge (m^3/s) is almost always flood-dominant (Fig. 5). This circumstance arises from the significant phase shift that occurs as the tide wave propagates up channel, resulting in a shorter flood period and thus higher peak discharge. From our measures of instantaneous discharge across seasons and tidal conditions, we calculate mean ebb and flood discharges (m^3/s) for each transect (Fig. 5). Mean discharge for the northern transect is ~9100 m^3/s on the flood and 8600 m^3/s on the ebb, and for the southern transect, mean flood and ebb discharges are ~14,600 and 14,200 m^3/s, respectively. From these results, we observe that mean discharge at the northern transect is again ~61±1% that of the southern transect, as also recognized for the tidal prism. Another notable result is that the mean flood discharge (m^3/s) is 3-6% greater than on the ebb tide, despite the tidal prism generally being ebb dominant. This disparity is a function of the shallow-water distortion of the M2 tide, which produces an asymmetrical waveform with a steeper rising limb than falling limb, and a corresponding reduction in the duration of the flooding tide by ~60-90 minutes.

4.3 – Hydrography – Sediment Transport:

Suspended sediment measurements collected during the hydrographic surveys show similar patterns to those of our long-term OBS station. Wet season sediment concentrations were generally 30-50% higher than during the dry season (Fig. 4). Much greater differences in SSC were observed, however, between neap and spring tidal conditions, with the latter concentrations being typically ~3 fold greater (0.3-1.5 g/L vs 0.1-0.5 g/L). These sediment concentrations, coupled with the water discharge observations, were then extrapolated over the tidal cycle to generate estimates of the rates and magnitude of sediment transport (Table 1). Results show that integrated sediment transport over a tidal limb varied by more than an order of magnitude at both transects. Minima of 0.16×10^8 kg (north) and 0.2×10^8 kg (south) were observed during the neap, dry-season ebb tide, and maxima of 3.3×10^8 kg (north) and 3.9×10^8 kg (south) occurred on the spring, monsoon flood tides. These values equate to mean rates of sediment transport that range from ~700 kg/s during neap, dry season conditions to ~17,000 kg/s during monsoon-season spring tides. Comparing the ebb and flood limbs of our surveys, the mean sediment discharge for the ebb tide is 5800 kg/s compared to 7800 kg/s for the flood tide, demonstrating an overall flood dominance in sediment transport.

These patterns are further supported by the net sediment transport values (i.e., ebb – flood; Table 1). For a given tidal cycle, net sediment transport was typically 10^6-10^7 kg, with magnitude varying largely with tidal phase, where spring tides generate 1.5 to 3 times

greater net transport than during neap tides (Table 1). Seasonally, net sediment transport rates were ~30% greater during the wet season, similar to our observations of suspended sediment concentration. Finally, a comparison of net sediment transport with corresponding net water discharge shows the two to covary, as expected, with greater net water discharge resulting in greater net sediment transport (Fig. 6). However, an important attribute of this relationship reveals a significant bias toward flood-dominant sediment transport. Data show that even neutral to weakly ebb dominant water discharge yields net transport in the flood direction (Fig. 6). As noted for water discharge (m^3/s), this disparity is a function of the non-negligible tidal components beyond M2 that result in a shortened flood limb and extended ebb period (Fig. 2; Table 1). Together, mean sediment discharge and net sediment transport patterns thus indicate an overall flood-oriented asymmetry and net onshore transport of sediment.

5 - Discussion

5.1 – Relative importance of tides and river

The GBM tidal delta plain comprises a complex channel network that has been little studied and will require substantial investigation to be understood well. Nevertheless, results of the current study allow for numerous observations on the scaling and magnitude of tidal mass transport within this region, establishing a baseline for the role that tides play in defining the delta system, particularly in the southwest region away from direct fluvial inputs. To begin, we take an average of the flood and ebb tidal prisms measured at the two sites on the Shibsa River over both spring and neap tidal phases during wet and dry seasons, and extrapolate the mean tidal prism over one year. In other words, an average of 2.7×10^8 m^3 water passes through this region on each of the ~705 tides per year. This basic estimation accounts for an average of $\sim 2 \times 10^{11}$ m^3 of water annually conveyed through our survey locations, 80 km inland of the coast. Furthermore, this mass exchange is principally tidal water, as the 50-75% of annual Gorai River discharge captured by the Shibsa River (i.e., $\sim 0.2 \times 10^{11}$ m^3) accounts for only 10% of the total water exchange observed for that channel.

The significance of these observations from the upstream Shibsa River tidal channel become more apparent when compared with the mainstem GBM rivers. In this case, the $\sim 2 \times 10^{11}$ m^3 of water conveyed annually through the upper Shibsa River is nearly 20% of the $\sim 11 \times 10^{11}$ m^3 of annual discharge from the entire GBM watershed (Lupker et al., 2011; Fig. 3). This is an impressive exchange of mass through the upper reaches of a single tidal channel along the GBM tidal delta plain. For context, the Shibsa River comprises approximately half (by planform area) of the Pussur River tidal system (Fig. 1), itself just one of five major tidal drainages along the GMB tidal delta plain (Fig. 1). Taken together, these basins include ~10 tidal channels having similar area (width × length) to the Shibsa River. We take the tidal flow through these systems to be broadly similar given the linear relationship between peak tidal discharge and the cross-sectional area of large tidal channels (Rinaldo et al., 1999), plus the fact that land-surface elevation and tidal range are

similar across the region (Chatterjee et al., 2013). Thus, even at a first-order, estimates of total mass transport across the tidal region would well exceed the $\sim 11 \times 10^{11}$ m^3 total volume discharged by the mainstem GBM rivers.

This comparable magnitude of tidal water exchange in the study area and the freshwater discharge of the GBM rivers demonstrates how tides hold comparable importance in controlling landscape development in the GBMD, which was suggested as far back as Galloway (1975). To consider geomorphic importance further, we make analogous estimations of sediment transport (Q_s) that supports land-surface aggradation and the dominant water discharge (Q_{dom}) that controls tidal channel morphology (Rinaldo et al., 1999). As done for water discharge, by taking the average of our tidal hydrography data for sediment transport we calculate a mean annual exchange of suspended sediment through the Shibsa River tidal station to be $\sim 1 \times 10^{11}$ kg ($\sim$100 Mt). For comparison, this estimate of sediment load is roughly 15% of the $\sim$700 Mt of sediment annually discharged to the coast by the GBM rivers (Goodbred and Kuehl, 1999). Thus, if we extrapolate any similar transport value to the other nine GBM tidal channels, then the sediment exchange through the tidal channels is easily found to be comparable to the main river mouth. There is, of course, the very important caveat that tidal sediment transport is not unidirectional, and so this integrated exchange of tidal sediment is not a net flux, as it is for the river sediment discharge. Nevertheless, the relevant point is that local, geomorphic reaches of the tidal delta plain have the opportunity for landscape building through tidal water and sediment exchange at a similar magnitude to the mainstem GBM rivers. This assertion is not surprising given the relative stability of the tidal delta plain, which experiences relatively little net erosion ($\sim$4 km^2/yr, or $\sim$0.02% annual loss; Sarwar and Woodroffe, 2013) and is offset by widespread sediment deposition on both land-surface (Rogers et al., 2013) and in channels (Wilson et al., 2017).

From this study, we understand that tidal energy, independent of the main river mouth, accounts for a twice-daily exchange of a mass equivalent to 4-15% of the yearly averaged daily GBM river discharge. In primary channels, the magnitude of this exchange is controlled more by the spring-neap tidal variability rather than the seasonal input of new material (Fig. 4). In the smaller BR channel, on the other hand, SSC variability demonstrates profound seasonality, presumably because discharge (and therefore stream power) is at least an order of magnitude smaller here than in the Shibsa River. This disparity is important when we consider land-building processes, as the majority of the SNF is plumbed by channels on the scale of the BR or smaller.

These findings emphasize the essential role that tides play in maintaining the largest portion of the GBM lower delta plain, which is not under direct river influence. However, despite the essential role of tides in sediment dispersal to large areas of the delta, the supply of sediment remains almost wholly derived from the river mouth and largely contemporaneous with seasonal fluvial discharge, especially in the secondary and tertiary channels that irrigate the SNF. Together, the coupled system in which the GBM rivers deliver sediment that is subsequently redistributed by tidal energy is fundamentally responsible for sustainability of this region relative to sea-level change. A significant

corollary of this fact is that a change in sediment supply from the GBM rivers, such as that proposed under the India River Linking Project, could pose a serious threat to delta sustainability (Higgins et al., 2018).

To summarize, as the central coastal region receives little direct water and sediment discharge from the GBM, the results herein emphasize that tidal exchange is the dominant geomorphic agent in the region with a mass and energy exchange of comparable or greater magnitude to the mainstem rivers. It is, of course, essential to recognize that most freshwater and sediment exchanged within the tidal system is ultimately sourced by the main rivers, and that these are intrinsically coupled systems. Thus, continued sustainability of the region will require the sustained delivery and exchange of water and sediment between the fluvial and tidal portions of the delta.

5.2 – Sedimentation in the Sundarbans and Infilling of Tidal Channels

Our observations of tidal sediment exchange provide a useful baseline for examining sedimentation in the Sundarbans and broader tidal delta plain, which are at risk from sea-level rise and inundation without an adequate supply of sediment. To date, the best estimate of total sedimentation in the Sundarbans is 1.1×10^{11} kg/year (~100 Mt), based on one season of direct sedimentation measures at 48 stations across the region (Rogers et al., 2013). This mass of sediment deposited in the Sundarbans is basically equivalent to the ~100 Mt of sediment that we observe transported through the Shibsa River transects. Thus, recalling that our local measurements likely capture just 5-10% of total suspended sediment transported through the tidal channels of the region, it becomes evident that there is generally adequate suspended sediment available to support regional sedimentation in the Sundarbans.

Another plausible implication is that there appears to be adequate sediment available for the restoration of land elevation within the poldered region, which is a major challenge facing coastal Bangladesh (Amir et al., 2013). Although a definitive answer remains to be determined, this general assertion is supported by observations of the rapid sedimentation that occurred on Polder 32 following embankment failures during cyclone Aila in 2009 (Auerbach et al., 2015). Measurements at Polder 32 after these failures found an average of 37±17 cm/yr of tidal sedimentation sustained over a two-year period, corresponding to a total annual deposition of ~5 Mt. Based on inundation depth and period, this accounts for an average of ~0.2 g/L for the water that flooded the island during this time. This value compares to a mean suspended sediment concentration of ~0.6 g/L measured during our hydrographic surveys, suggesting that roughly one-third of the tidal sediment inundating the landscape generated these very rapid sedimentation rates. Ultimately, limitations in the present data preclude a closed, precise sediment budget, but our collective observations over several different studies remain consistent in direction and magnitude. These indicate persistent, relatively rapid, rates of deposition that are sustained by the large-magnitude conveyance of sediment through the tidal channels and ultimately supplied by seasonal discharge of the mainstem rivers (Rogers et al., 2013; Auerbach et al., 2015; this study).

Upstream of our transect sites, the landscape is almost entirely embanked by polder systems. With limited opportunity for sediment deposition on this formerly intertidal platform, and with the resulting reduction in the tidal prism upstream, channel sedimentation and infilling has become a major problem. Wilson et al. (2017) demonstrate that by preventing the inundation of the intertidal platform, poldering has reduced the tidal prism of the broader southwest region by as much as 1.4×10^9 m^3. If we assume that this volume reduction is relatively evenly dispersed across the delta plain, then it would have led to a 25-50% reduction in the local tidal prism measured at our sites. These effects are at least partially responsible for the ~1400 km of channel infilling that has taken place over the last few decades, resulting in the creation of new agriculture and aquaculture opportunities but also altering drainage, transportation routes, and feedback responses of the regional tidal hydrodynamics (Wilson et al., 2017). The mass of sediment that has infilled these channels is calculated to be 6.15×10^{11} kg, which would be $\sim 1.2 \times 10^{10}$ kg/yr assuming a roughly constant rate (Wilson et al., 2017). Of these infilled channels, ~15% (~200 km) are part of the former channel network connecting upstream of our northern transect (Fig. 1). Thus, a proportional rate of sedimentation lost to these channels would be $\sim 0.18 \times 10^{10}$ kg/yr, which is ~25% of the estimated 0.68×10^{10} kg fluxing through the northern transect (to the north) each year. While this sediment flux is four times greater than the expected total based on infilling rates from Wilson et al. (2017), it relies on the same previously described assumptions (i.e., no lateral exchange with neighboring rivers, non-end-member flux reflecting an average of end-member conditions). More importantly, it appears that there is sufficient sediment available to continue infilling channels, and future studies should constrain whether this region is, in fact, infilling faster than other areas on the tidal delta plain, as this would hold important implications for regional navigation and hydrodynamic changes.

6 – Conclusions

In the present study, we have measured tidal and seasonal variability associated with water discharge and suspended sediment concentration (SSC), and used these observations to compute the magnitude of water and sediment exchange through a single tidal channel. As has been suggested previously, the wet season is found to exert a strong control on the timing and magnitude of sediment transport in this system, despite seemingly modest changes to the hydrodynamics. Indeed, despite a reduced tidal range and similar peak SSC, sediment transport during the monsoon is always of greater magnitude than during the dry season. Understanding this relationship is critical for planning any potential land recovery strategies in the future. The importance of the monsoon also provides a new perspective into the meaning of a "tidal delta." While it is clearly the tides that perform much of the work to shape the delta – including driving a net flood-oriented direction of sediment flux – it is the seasonal influx of riverine sediment that allows this work to continue. Finally, this research demonstrates that the mass of sediment transported north of our study area is more than sufficient to fill channels and create additional land. Ideally, future land-use management strategies should divert some of this excess sediment into polder interiors through tidal river management, and allow this landscape to continue to prosper.

Code availability:

Data availability:
Data used for this publication will be archived in the Marine Geoscience Data System.

Sample availability:
Samples from this publication are stored in the sedimentology laboratory at Vanderbilt University

Author Contribution:
The experiment was designed by RH and SG, with input from RB and JB. RH and RB lead the field research efforts with support from SG and JB. RH wrote the majority of the manuscript and figures, with substantial input from SG. RB and JB also contributed to the manuscript and figures.

Competing interests:
The authors declare that they have no conflict of interest.

Acknowledgements:
This work would not be possible without the support of our local collaborators, Drs. Kazi Matin Ahmed and Syed Humayun Akchter from Dhaka University, who oversee in-country logistics and offer local guidance. We would also like to thank Abu Naser Hossain of the Forestry Crime Department for his help with permitting, and Nasrul Islam Bachchu of Pugmark Tours, and the captain and crew of the M/V Bawali and M/L Mawali for their seemingly endless patience with our field logistics. We would also like to thank Md. Saddam Hossain, Abrar Hossain, Mynul Hassan, Carol Wilson, and Mike Reed for their field support. This research was supported by the US Office of Naval Research (N00014-11-1-0683) and the National Science Foundation (Coastal SEES- #1600319).

References:

Ali, A., Mynett, A.E. and Azam, M.H. Sediment dynamics in the Meghna estuary, Bangladesh: A model study. Journal of Waterway Port Coastal and Ocean Engineering-ASCE, 133: 255-263, 2007.

Allison, M. and Kepple, E. Modern sediment supply to the lower delta plain of the Ganges-Brahmaputra River in Bangladesh. *Geo-Marine Letters*, *21*(2), pp.66-74, 2001.

Alongi, D.M. Carbon cycling and storage in mangrove forests. *Annual review of marine science*, *6*, pp.195-219, 2014.

Amir, M.S.I.I., Khan, M.S.A., Khan, M.K., Rasul, M.G. and Akram, F. Tidal river sediment management-A case study in southwestern Bangladesh. *International Journal of Environmental, Chemical, Ecological, Geological and Geophysical Engineering*, *7*(3), pp.176-185, 2013.

Anthony, E.J., Brunier, G., Besset, M., Goichot, M., Dussouillez, P. and Nguyen, V.L. Linking rapid erosion of the Mekong River delta to human activities. *Scientific reports*, *5*, p.14745, 2015.

Auerbach, L.W., Goodbred Jr, S.L., Mondal, D.R., Wilson, C.A., Ahmed, K.R., Roy, K., Steckler, M.S., Small, C., Gilligan, J.M. and Ackerly, B.A. Flood risk of natural and embanked landscapes on the Ganges–Brahmaputra tidal delta plain. *Nature Climate Change*, *5*(2), p.153, 2015.

Ayers, J. C., George, G., Fry, D., Benneyworth, L., Wilson, C., Auerbach, L., Roy, K., Karim, M.R., Akter, F.. Goodbred, S. Salinization and arsenic contamination of surface water in southwest Bangladesh. *Geochemical Transactions*, *18*(1), 4, 2017.

Barua, D. K., Kuehl, S. A., Miller, R. L., & Moore, W. S. Suspended sediment distribution and residual transport in the coastal ocean off the Ganges-Brahmaputra river mouth. *Marine Geology*, *120*(1-2), 41-61, 1994.

Brammer, H. Bangladesh's dynamic coastal regions and sea-level rise. *Climate Risk Management*, *1*, pp.51-62, 2014.

Brown, J.M. and Davies, A.G. Flood/ebb tidal asymmetry in a shallow sandy estuary and the impact on net sand transport. *Geomorphology*, *114*(3), pp.431-439, 2010.

Brown, S. and Nicholls, R.J. Subsidence and human influences in mega deltas: the case of the Ganges–Brahmaputra–Meghna. *Science of the Total Environment*, *527*, pp.362-374, 2015.

Chatterjee, M., Shankar, D., Sen, G.K., Sanyal, P., Sundar, D., Michael, G.S., Chatterjee, A., Amol, P., Mukherjee, D., Suprit, K. and Mukherjee, A. Tidal variations in the Sundarbans estuarine system, India. *Journal of earth system science*, *122*(4), pp.899-933, 2013.

Darby, S.E., Hackney, C.R., Leyland, J., Kummu, M., Lauri, H. Parsons, D.R., Best, J.L, Nicholas, A.P. and Aalto, R. Fluvial sediment supply to a mega-delta reduced by shifting tropical-cyclone activity. *Nature*, 539, 276-279, doi:10.1038/nature19809, 2016.

Darby, S.E., Nicholls, R.J., Rahman, M.M., Brown, S. and Karim, R. A Sustainable Future Supply of Fluvial Sediment for the Ganges-Brahmaputra Delta. In *Ecosystem Services for Well-Being in Deltas* (pp. 277-291). Palgrave Macmillan, Cham, 2018.

Ericson, J.P., Vörösmarty, C.J., Dingman, S.L., Ward, L.G. and Meybeck, M. Effective sea-level rise and deltas: causes of change and human dimension implications. *Global and Planetary Change*, *50*(1-2), pp.63-82, 2006.

670 Galloway, W.E. Process framework for describing the morphologic and stratigraphic
671 evolution of deltaic depositional systems, 1975.
672 Goodbred Jr, S.L. and Kuehl, S.A. Holocene and modern sediment budgets for the Ganges-
673 Brahmaputra river system: Evidence for highstand dispersal to flood-plain, shelf, and
674 deep-sea depocenters. *Geology*, *27*(6), pp.559-562, 1999.
675 Grinsted, A. Tidal fitting toolbox (v 1.3.0.0), Matlab code,
676 https://www.mathworks.com/matlabcentral/fileexchange/19099-tidal-fitting-
677 toolbox?s_tid=srchtitle, 2008.
678 Higgins, S.A., Overeem, I., Steckler, M.S., Syvitski, J.P., Seeber, L. and Akhter, S.H. InSAR
679 measurements of compaction and subsidence in the Ganges-Brahmaputra Delta,
680 Bangladesh. *Journal of Geophysical Research: Earth Surface*, *119*(8), pp.1768-1781,
681 2014.
682 Higgins, S., Overeem, I., Rogers, K. and Kalina, E. River linking in India: Downstream impacts
683 on water discharge and suspended sediment transport to deltas. *Elem Sci Anth*, *6*(1),
684 2018.
685 Hossain, M.S., Dearing, J.A., Rahman, M.M, and Salehin, M. Recent changes in ecosystem
686 services and human well-being in the Bangladesh coastal zone. Regional
687 Environmental Change 16(2):429-443, 2016.
688 Islam, M.R. 18 Managing Diverse Land Uses in Coastal Bangladesh: Institutional
689 Approaches. *Environment and livelihoods in tropical coastal zones*, p.237, 2006.
690 Kamal, A.S.M., Hossain, A., Hossain, B.M., Hassan, S.M. and Rashid, A.K.M. Physical and Social
691 Assessment of the Waterlogged Area and Suitability of the "Inclusive and Adaptive
692 Tidal River Management Technique" to Alleviate Waterlogging in Southwest
693 Bangladesh. *Procedia engineering*, *212*, pp.760-767. , 2018.
694 Khadim, F.K., Kar, K.K., Halder, P.K., Rahman, M.A. and Morshed, A.M. Integrated water
695 resources management (IWRM) impacts in south west coastal zone of Bangladesh and
696 fact-finding on tidal river management (TRM). *Journal of Water Resource and*
697 *Protection*, *5*(10), p.953, 2013.
698 Marois, D.E. and Mitsch, W.J. Coastal protection from tsunamis and cyclones provided by
699 mangrove wetlands–a review. *International Journal of Biodiversity Science, Ecosystem*
700 *Services & Management*, *11*(1), pp.71-83, 2015.
701 Mcleod, E., Chmura, G.L., Bouillon, S., Salm, R., Björk, M., Duarte, C.M., Lovelock, C.E.,
702 Schlesinger, W.H. and Silliman, B.R. A blueprint for blue carbon: toward an improved
703 understanding of the role of vegetated coastal habitats in sequestering CO2. *Frontiers*
704 *in Ecology and the Environment*, *9*(10), pp.552-560, 2011.
705 Nowreen, S., Jalal, M.R. and Khan, M.S.A. Historical analysis of rationalizing South West
706 coastal polders of Bangladesh. *Water Policy*, *16*(2), pp.264-279, 2014.
707 Ogston, A.S. and Sternberg, R.W. Sediment-transport events on the northern California
708 continental shelf. *Marine Geology*, *154*(1-4), pp.69-82, 1999.
709 Overeem I. and Syvitski, J.P.M. Dynamics and Vulnerability of Delta Systems: LOICZ Reports
710 and Studies, No 35, GKSS Research Center, Geesthacht, 54 p., 2009.
711 Pendleton, L., Donato, D.C., Murray, B.C., Crooks, S., Jenkins, W.A., Sifleet, S., Craft, C.,
712 Fourqurean, J.W., Kauffman, J.B., Marbà, N. and Megonigal, P. Estimating global "blue
713 carbon" emissions from conversion and degradation of vegetated coastal
714 ecosystems. *PloS one*, *7*(9), p.e43542, 2012.

715 Pethick, J.S. Velocity surges and asymmetry in tidal channels. *Estuarine and Coastal Marine*
716 *Science*, *11*(3), pp.331-345, 1980.
717 Pethick, J. and Orford, J.D. Rapid rise in effective sea-level in southwest Bangladesh: its
718 causes and contemporary rates. *Global and Planetary Change*, *111*, pp.237-245, 2013.
719 Rinaldo, A., Fagherazzi, S., Lanzoni, S., Marani, M. and Dietrich, W.E. Tidal networks: 3.
720 Landscape-forming discharges and studies in empirical geomorphic
721 relationships. *Water Resources Research*, *35*(12), pp.3919-3929, 1999.
722 Rogers, K.G., Goodbred Jr, S.L. and Mondal, D.R. Monsoon sedimentation on the 'abandoned'
723 tide-influenced Ganges–Brahmaputra delta plain. *Estuarine, Coastal and Shelf*
724 *Science*, *131*, pp.297-309, 2013.
725 Sakib, M., Nihal, F., Haque, A., Rahman, M., & Ali, M. Sundarban as a Buffer against Storm
726 Surge Flooding. *World Journal of Engineering and Technology*, *3*, 59–64, 2015.
727 Sarwar, M.G.M. and Woodroffe, C.D. Rates of shoreline change along the coast of
728 Bangladesh. *Journal of Coastal Conservation*, *17*(3), pp.515-526, 2013.
729 Shaha, D.C. and Cho, Y.K. Salt plug formation caused by decreased river discharge in a
730 multi-channel estuary. *Scientific reports*, *6*, p.27176, 2016.
731 Steckler, M.S., Nooner, S.L., Akhter, S.H., Chowdhury, S.K., Bettadpur, S., Seeber, L. and
732 Kogan, M.G. Modeling Earth deformation from monsoonal flooding in Bangladesh using
733 hydrographic, GPS, and Gravity Recovery and Climate Experiment (GRACE)
734 data. *Journal of Geophysical Research: Solid Earth*, *115*(B8) , 2010.
735 Syvitski, J.P. Supply and flux of sediment along hydrological pathways: research for the 21st
736 century. *Global and Planetary Change*, *39*(1-2), pp.1-11, 2003.
737 Syvitski, J.P. and Milliman, J.D. Geology, geography, and humans battle for dominance over
738 the delivery of fluvial sediment to the coastal ocean. *The Journal of Geology*, *115*(1),
739 pp.1-19, 2007.
740 Syvitski, J.P. Deltas at risk. *Sustainability Science*, *3*(1), pp.23-32, 2008.
741 Syvitski, J.P., Kettner, A.J., Overeem, I., Hutton, E.W., Hannon, M.T., Brakenridge, G.R., Day, J.,
742 Vörösmarty, C., Saito, Y., Giosan, L. and Nicholls, R.J. Sinking deltas due to human
743 activities. *Nature Geoscience*, *2*(10), p.681, 2009.
744 Uddin, M. S., van Steveninck, E. D. R., Stuip, M., & Shah, M. A. R. Economic valuation of
745 provisioning and cultural services of a protected mangrove ecosystem: a case study on
746 Sundarbans Reserve Forest, Bangladesh. *Ecosystem Services*, *5*, 88-93, 2013.
747 Wilson, C., Goodbred, S., Small, C., Gilligan, J., Sams, S., Mallick, B. and Hale, R. Widespread
748 infilling of tidal channels and navigable waterways in human-modified tidal deltaplain
749 of southwest Bangladesh. *Elem Sci Anth*, *5*, 2017.
750 Winterwerp, J.C. and Giardino, A. Assessment of increasing freshwater input on salinity and
751 sedimentation in the Gorai river system. *World Bank Project*, pp.1206292-000, 2012.
752 Yan, W. Can mangroves buffer ocean acidification?, *Eos, 97,* 2016.
753
754
755
756
757

Earth Surf. Dynam. Discuss., https://doi.org/10.5194/esurf-2018-66
Manuscript under review for journal Earth Surf. Dynam.
Discussion started: 19 September 2018

Table 1: Measurements of sediment flux and tidal prism from the Shibsa River. Shaded rows represent measurements taken during spring tides.

	Transect	Tidal Range (m)	Tidal Prism (m^3)			Sediment Load (kg)		
			Ebb	Flood	Net	Ebb	Flood	Net
Dry Season	South	2.1	2.00E+08	-2.00E+08	4.30E+05	2.05E+07	-4.70E+07	-2.66E+07
	North	2.2	1.40E+08	-1.50E+08	-1.30E+07	1.55E+07	-2.37E+07	-8.21E+06
	South	5.5	4.50E+08	-4.30E+08	2.30E+07	1.83E+08	-2.30E+08	-4.69E+07
	North	5.7	3.10E+08	-2.30E+08	7.90E+07	2.15E+08	-1.90E+08	2.49E+07
Monsoon	South	2.7	2.64E+08	-1.81E+08	8.28E+07	4.47E+07	-3.89E+07	5.77E+06
	North	2.2	1.83E+08	-1.06E+08	7.69E+07	6.20E+07	-4.12E+07	2.08E+07
	South	4	4.71E+08	-5.12E+08	-4.16E+07	3.20E+08	-3.85E+08	-6.50E+07
	North	3.9	2.40E+08	-2.85E+08	-4.43E+07	2.54E+08	-3.31E+08	-7.65E+07

Earth Surf. Dynam. Discuss., https://doi.org/10.5194/esurf-2018-66
Manuscript under review for journal Earth Surf. Dynam.
Discussion started: 19 September 2018

764 **Figures:**

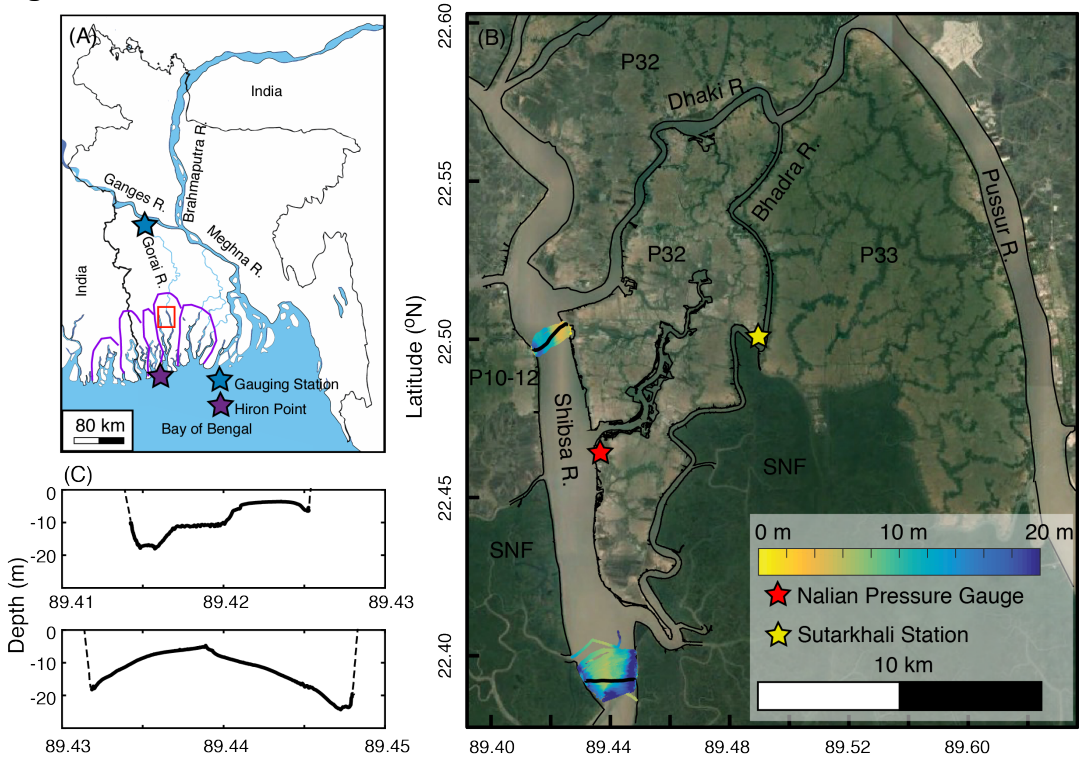

765
766 Fig. 1 – A) Location of Bangladesh and the specific region of interest for this study, as well
767 as the approximate outlines of the five major tidal distributary basins of the SW delta in
768 purple. B) Satellite image of P-32 study area, with bathymetry overlain in the regions of the
769 northern and southern transects. Long-term and short-term pressure sensor locations are
770 also identified. C) Characteristic river cross sections for the northern and southern
771 transects. The specific transects used for these cross sections are highlighted in black in
772 (B).

Earth Surf. Dynam. Discuss., https://doi.org/10.5194/esurf-2018-66
Manuscript under review for journal Earth Surf. Dynam.
Discussion started: 19 September 2018

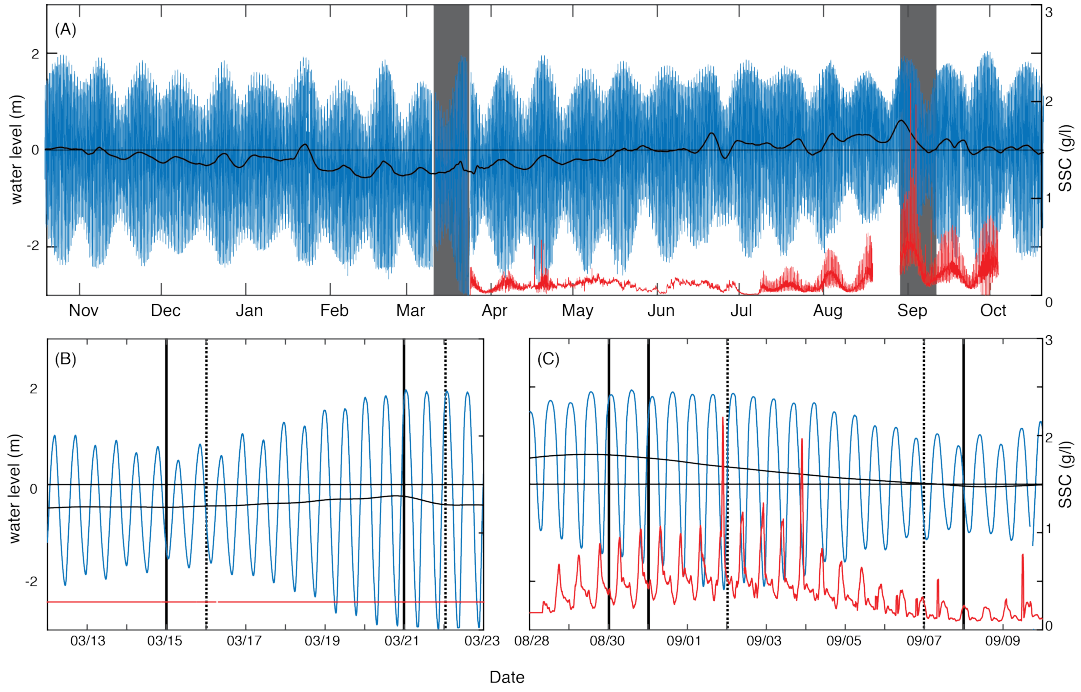

Fig. 2 – A) Long-term water level elevation (blue) and suspended sediment concentration (red) recorded at Sutarkhali. Black is the tidally filtered water level to highlight seasonal trends of relatively higher water during the monsoon, despite similar maximum tidal elevation. Note also the arrival of increased SSC associated with monsoon discharge of the GBM, beginning in August. Areas shaded in gray depict the periods of focused field work, highlighted below in panels (B) and (C). Days where transect measurements were recorded are noted with vertical black lines, where solid are from the southern transect, and dashed are from the northern transect. In (B), the horizontal red line represents the maximum SSC observed in the spring-neap tidal cycle following our focused field work, as SSC was not measured at this location previously.

Earth Surf. Dynam. Discuss., https://doi.org/10.5194/esurf-2018-66
Manuscript under review for journal Earth Surf. Dynam.
Discussion started: 19 September 2018

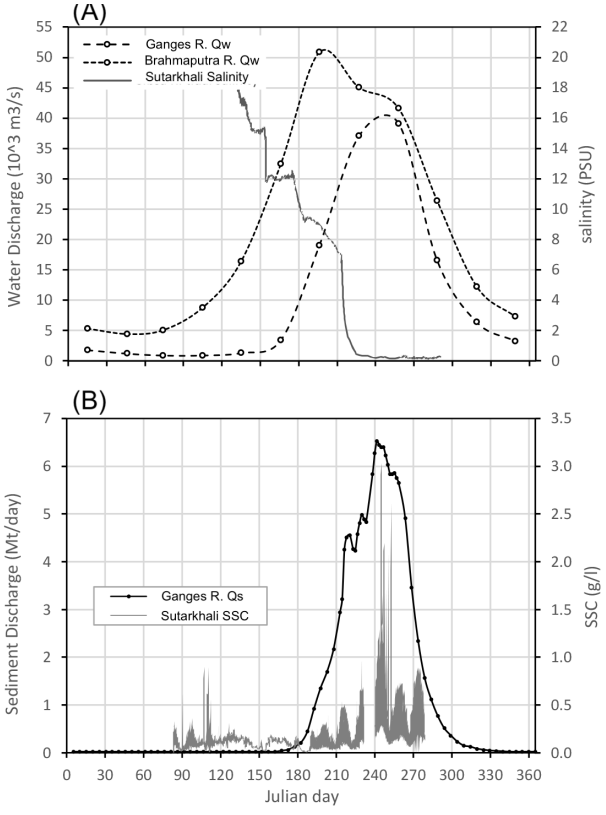

Fig. 3 – A) Ganges and Brahmaputra River water discharge (Qw), and salinity measured at Sutarkhali Station, demonstrating the reduction in P-32 salinity associated with the arrival of freshwater from the GBM rivers. B) Ganges river sediment discharge (Qs) and SSC measured at Sutarkhali station, demonstrating the increase in local SSC coincident with the peak SSC discharge of the Ganges R.

Earth Surf. Dynam. Discuss., https://doi.org/10.5194/esurf-2018-66
Manuscript under review for journal Earth Surf. Dynam.
Discussion started: 19 September 2018

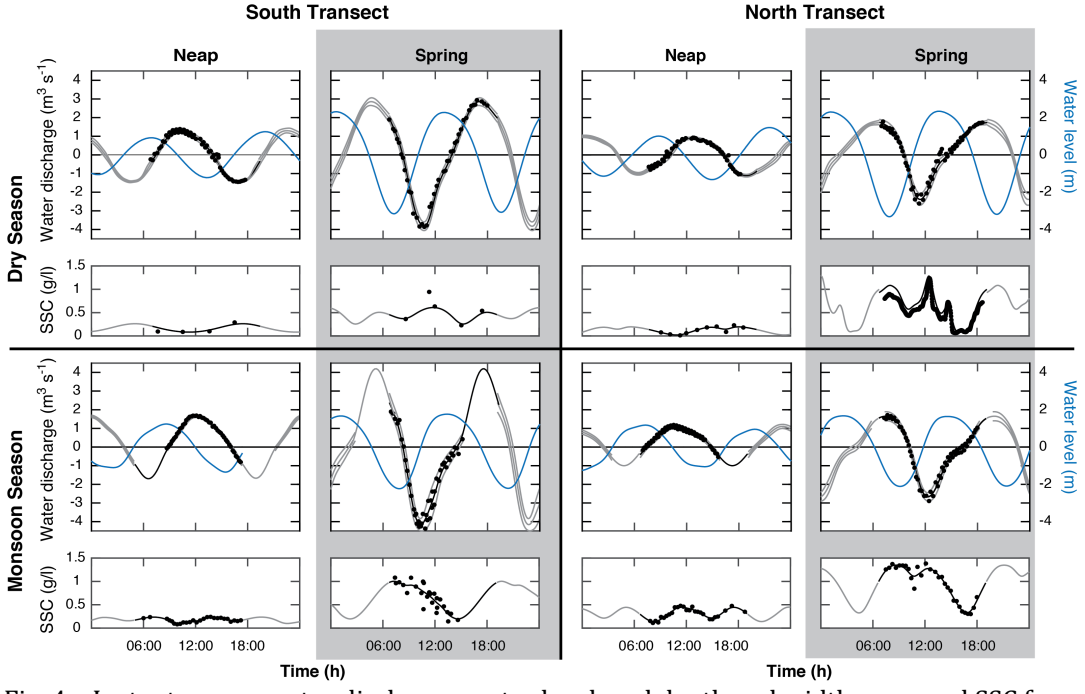

Fig. 4 – Instantaneous water discharge, water level, and depth and width-averaged SSC for each day of cross-channel transects. Dry season measurements are in the upper half, while monsoon season transects are on the bottom. Spring tides in either season are shaded in gray. The two left columns are southern measurements, and the two right columns are from the northern transect. Black dots correspond to specific measurements, while gray lines represent the estimated error, tile forwards and backwards by 12.4 hours. For discharge, dashed lines in the monsoon represent maxima based on extrapolations from the dry season ratio. While seemingly unreasonable, they are provided here for context.

Earth Surf. Dynam. Discuss., https://doi.org/10.5194/esurf-2018-66
Manuscript under review for journal Earth Surf. Dynam.
Discussion started: 19 September 2018

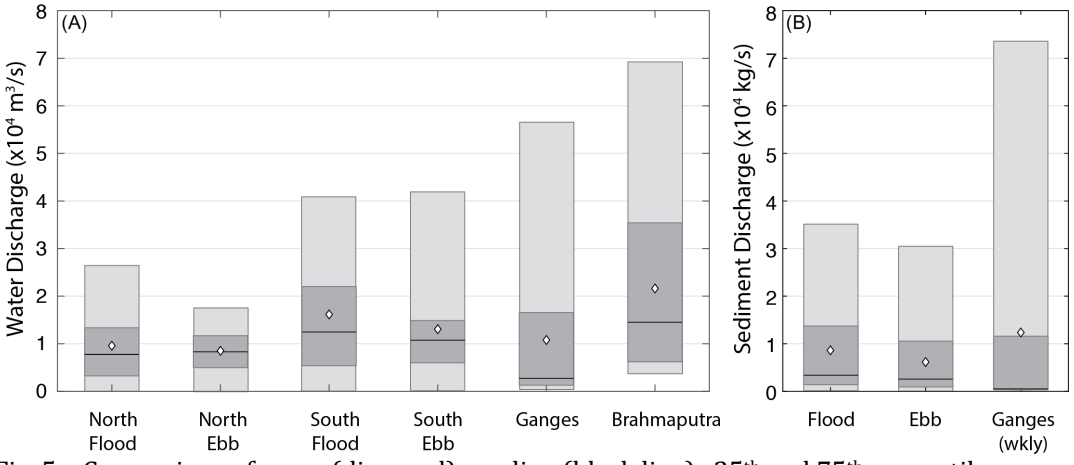

Fig. 5 – Comparison of mean (diamond), median (black line), 25th and 75th percentile (lower and upper limits of darkly shaded box) and total range (lightly shaded box) for water discharge (A), and sediment discharge (B). A) demonstrates that median and mean discharge along either transect are comparable to those of either the Ganges or Brahmaputra River. B) demonstrates that as with water, mean sediment discharge on both the flood and ebb tides is approximately the same as the weekly averaged Ganges sediment discharge.

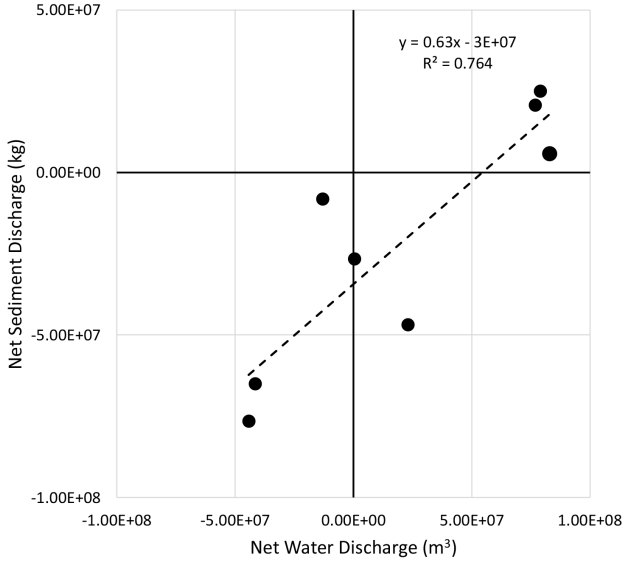

Fig. 6 – Net water discharge vs. net sediment discharge for all of the survey days on the Shibsa River. As expected, we observe a positive trend to this relationship. The negative y-intercept of the best-fit curve demonstrates the overall flood-oriented nature of sediment transport in this tidal channel.